A TWO-DIMENSIONAL STEADY-STATE SIMULATION MODEL FOR A LEAD BLAST FURNACE

Peter VERGUTS, Bart BLANPAIN and Patrick WOLLANTS

Department of Metallurgy and Materials Engineering (MTM), K.U.Leuven

Kasteelpark Arenberg 44, B-3001 Heverlee (Leuven), Belgium

ABSTRACT

The complex interaction between the phenomena occurring in the blast furnace makes mathematical simulation a useful tool to study this process and improve its performance. In this paper a two-dimensional steady-state simulation model for a lead blast furnace is presented, that includes flow models for the gas, solid and liquid phase, together with a chemical reaction sub-model and a heat transfer sub-model. The influence of certain process parameters such as oxygen enrichment of the blast air and blast temperature on the in-furnace phenomena is investigated using this model. An outline of the model as well as some interesting results will be presented.

NOMENCLATURE

a_i	specific surface of phase i	$(1/m)$
c_{pi}	specific heat of phase i	$(J/kg \cdot K)$
d_p	diameter of particles	(m)
G_{ij}	mass velocity of phase i in direction j	$(kg/m^2 \cdot s)$
h_{ij}	convective heat transfer coefficient between phases i and j	$(W/m^2 \cdot K)$
mf_i	mass fraction of component i	$(-)$
M_i	molar mass of component i	$(g/mole)$
P	pressure	(Pa)
$R_k{}^*$	rate of reaction R_k	$(mole/m^3 \cdot s)$
T_i	temperature of phase i	(K)
V_{ij}	superficial velocity of phase i in direction j	(m/s)
ε	permeability of the packed bed	$(-)$
$\eta_{k,i}$	fraction of reaction heat of reaction k that is attributed to phase i	$(-)$
ϕ	shape factor	$(-)$
χ_{ik}	stoichiometric coefficient for species i in reaction k	$(-)$
ρ_i	density of phase i	(kg/m^3)
μ_g	dynamic viscosity	$(kg/m \cdot s)$
ΔH_k	reaction heat of reaction R_k	$(J/mole)$

INTRODUCTION

Numerical modeling is increasingly applied for improving knowledge and control of complex processes in metallurgy. In recent years many models of the iron blast furnace process have been published in literature. The most impressive model is undoubtedly the multi-fluid model of Yagi (Austin et al., 1997; de Castro et al., 2000; Akiyama et al., 2000; de Castro et al., 2002). The same evolution however has not occurred with regard to modeling of the lead blast furnace process. Only a few models of a lead blast furnace are available in literature (Cowperthwaite et al., 1980; Chao, 1981; Hussain and Morris, 1989). An evident reason for this is the lower economic importance of the latter process. The current research is a first attempt to close the gap to some extent.

THE LEAD BLAST FURNACE PROCESS

The lead blast furnace process is quite similar to the iron blast furnace process. The burden, which is charged at the top, consists mainly of coke, lead containing raw materials and fluxes. At the bottom of the furnace, oxygen enriched air is blown into the packed bed. The combustion reactions between the oxygen of the blast air and the carbon in the coke supply the necessary heat to melt the charge. The CO-gas that is formed during these combustion reactions, rises in the shaft of the furnace and reduces part of the oxides in the burden. This is called indirect reduction. The part of the oxidic materials in the charge that melts before it is reduced flows over the solid coke and is thus reduced by the solid carbon. This is called direct reduction. One of the main differences between the lead and iron blast furnace is the geometry. Apart from being much smaller, a lead blast furnace has a rectangular cross-section (see geometry of the furnace in figure 1), whereas the iron blast furnace has a circular cross-section. In the iron blast furnace high CO/CO_2-ratios are necessary to reduce the iron oxides. In the lead blast furnace high CO/CO_2-ratios should be avoided to prevent the iron oxides present from being reduced. This is achieved by the small distance between the opposed blast air nozzles.
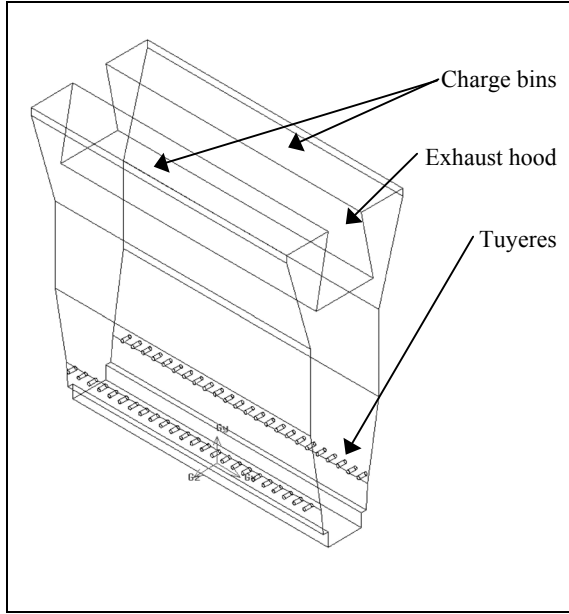
Figure 1: Geometry of the lead blast furnace.

MODEL DESCRIPTION

Introduction: overview of the global model

Figure 2 illustrates how the global model is subdivided into sub-models. The complex interactions between the different phenomena are reflected in the model by the coupled nature of the mathematical equations. This necessitates an iterative solution approach, which is shown in figure 2. In the next sections, the different sub-models will be discussed.
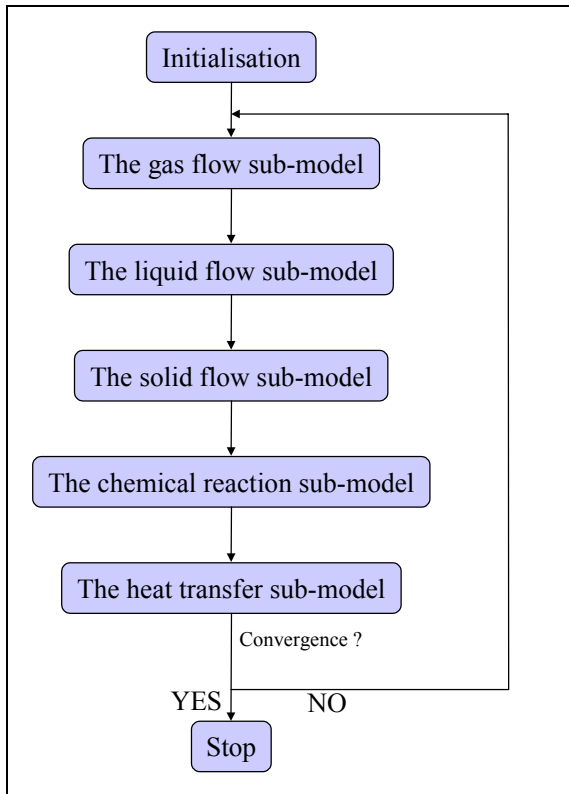

Figure 2: Schematic view of the global model.

The gas flow sub-model

The main variables that are solved in this sub-model are the mass velocities in x and y direction, G_{gx} and G_{gy}, together with the pressure P. Ergun's equation is used in its two-dimensional form, which is given by:

$$\frac{\partial P}{\partial x} = -f_1 G_{gx} - f_2 \left| \vec{G} \right| G_{gx} \qquad (1)$$

$$\frac{\partial P}{\partial y} = -f_1 G_{gy} - f_2 \left| \vec{G} \right| G_{gy} \qquad (2)$$

with

$$f_1 = \frac{150(1-\varepsilon)^2 \mu_g}{\rho_g (\phi d_p)^2 \varepsilon^3}$$

$$f_2 = \frac{1.75(1-\varepsilon)}{\rho_g (\phi d_p) \varepsilon^3}$$

Beside the Ergun equations, also the continuity equation for the gas phase is solved in this sub-model:

$$\frac{\partial G_{gx}}{\partial x} + \frac{\partial G_{gy}}{\partial y} = \sum_{k=1}^{N} \beta_k R_k^* \qquad (3)$$

with

$$\beta_k \equiv \sum_{i=1}^{n} (\chi_{ik} M_i)_g$$

There are thus three equations for the three variables P, G_{gx} and G_{gy}. As boundary conditions the flow rate is specified at the nozzle inlets, atmospheric pressure is imposed at the charge bin boundaries and a constant underpressure is specified at the exhaust hood. The surface of the liquid bath is set as a wall for the gas phase.

The solid flow sub-model

In this sub-model the flow of the solids in the burden is calculated. The variables that have to be calculated are V_{sx} and V_{sy}. One equation that can readily be used is the continuity equation for the solid phase, which is given by:

$$\frac{\partial(\rho_s V_{sx})}{\partial x} + \frac{\partial(\rho_s V_{sy})}{\partial y} = \sum_{k=1}^{N} \beta_k R_k^* \qquad (4)$$

For the second equation, it is assumed in this model that the solid flow is irrotational, resulting in the following additional equation:

$$\frac{\partial V_{sy}}{\partial x} - \frac{\partial V_{sx}}{\partial y} = 0 \qquad (5)$$

Velocity normal to the walls is set to zero, and furthermore, the bottom of the furnace is treated as a wall, meaning that no solid material leaves the hearth. The solid flow field is thus completely dependent on the reactions that occur in the blast furnace. The production rate can therefore be easily calculated by integrating solid mass flow over the inlets of the charge bins.

The liquid flow sub-model

The continuity equation for the liquid flow is given by:

$$\frac{\partial(\rho_l V_{lx})}{\partial x} + \frac{\partial(\rho_l V_{ly})}{\partial y} = \sum_{k=1}^{N} \beta_k R_k^* \qquad (6)$$

As in the solid flow sub-model, an additional equation is required to calculate the variables V_{lx} and V_{ly}. In this

model it is assumed that the fluid flows straight down, except at inclined walls, where velocities are assumed parallel to the walls. In the present model, drag forces caused by gas flow are not incorporated. This effect will be large in front of the nozzles where the gas will push the liquid droplets to the middle of the furnace. Furthermore these drag forces can be responsible for the phenomenon of flooding. Including these drag forces in the model will be part of further work.

The chemical reaction sub-model

The blast furnace is a metallurgical reactor in which numerous reactions occur at different locations in the furnace. In this sub-model the rate of every reaction is calculated for every cell using the most recent values for the parameters that are used in the reaction rate equations. At this point only the following reactions are included in the model:

$C(s) + O_2(g) \rightarrow CO_2(g)$	R_1
$C(s) + CO_2(g) \rightarrow 2CO(g)$	R_2
$PbO(s) \rightarrow PbO(l)$	R_3
$PbO(l) + C(s) \rightarrow Pb(l) + CO(g)$	R_4

Table 1: Reactions in the lead blast furnace.

The first reaction is the combustion reaction of the coke. This reaction occurs immediately in front of the tuyeres. The second reaction is the so-called Boudouard reaction. It occurs throughout the furnace, but its rate is higher in the high temperature region of the furnace. The third reaction is the melting reaction of PbO. The last reaction describes the direct reduction reaction of the liquid lead oxide with the solid coke. At this point, indirect reduction is neglected since the main feed materials have low porosity. In the chemical reaction sub-model the composition of the different phases is also recalculated. In order to do this, a separate continuity equation has to be solved for every component. For the solid phase, consisting of PbO and C, the continuity equations can be written as:

$$\nabla(mf_{PbO} \cdot \rho_s \overrightarrow{V_s}) = -M_{PbO} R_3^* \qquad (7)$$

$$\nabla(mf_C \cdot \rho_s \overrightarrow{V_s}) = -M_C \left(R_1^* + R_2^* + R_4^* \right) \qquad (8)$$

The sum of these continuity equations should result in the global continuity equation of that phase. Similar equations are used for the gas and liquid phase composition.

The heat transfer sub-model

In the heat transfer sub-model, the temperatures of the different phases are calculated. In the present model conductive and radiative heat transfer are neglected. The heat transfer equations are thus reduced to:

$$\nabla\left(c_{p_i} T_i \rho_i \overrightarrow{V_i}\right) + \sum_{i \neq j} h_{ij} a_i \left(T_i - T_j\right) = \\ \sum_k \eta_{k,i} R_k^* \left(-\Delta H_k\right) \qquad (9)$$

The heat transfer coefficient between the gas and solid phases is calculated using an expression by Stuke (Stuke,

1948) that correlates the overall parameter to the true film heat transfer coefficient (h_{gs}') and the conductivity of the solid phase (k_s):

$$\frac{1}{h_{gs}} = \frac{1}{h_{gs}'} + \frac{d_p}{10} k_s \qquad (10)$$

For the true heat transfer coefficient, h_{gs}', a correlation by Shirai (Shirai, 1953) was used:

$$\varepsilon\left(\frac{h_{gs}' d_p}{k_g}\right) = 2.0 + 0.75 \, Pr^{1/3} \, Re_p^{1/2} \qquad (11)$$

in which Pr and Re_p refer to the Prandtl and particle Reynolds number respectively. Heat transfer coefficients between gas and liquid phase, and liquid and solid phase, are at this point arbitrarily chosen constants. More accurate correlations will be part of further work.

The mesh

In the current state of the model a very simple rather coarse grid is used that consists of rectangular cells. The coarse grid is used because the model is still more or less in a development stage, which makes calculation speed somewhat more important than precise results. The meshes for the gas, solid and liquid phase have minor differences. Figure 3 shows the mesh for the solid phase; the cells are represented by squares which deforms the true geometry of the blast furnace a bit.
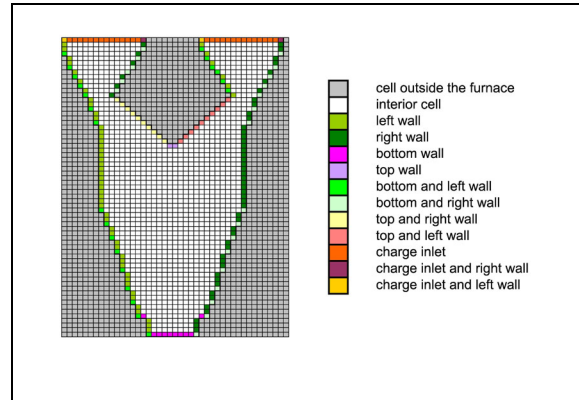

Figure 3: Schematic view of the mesh for the solid phase.

RESULTS

In a first section the results of a base case will be discussed. The information that can be obtained from the model will be presented. In following sections the influence of certain operating parameters on blast furnace operation will be discussed.

The base case

Table 3 shows the different parameters that were used to model the base case. For a clear understanding of the results that will be presented, it is necessary to have a clear view of the flow fields of the different phases. Figure 4 gives a global view of the gas flow in the blast furnace. The gas enters the furnace at high velocity and initially flows in all directions. The gas speed rapidly declines in the furnace. Because of the lower pressure at the exhaust hood boundary, compared with the atmospheric pressure at the charge bins, so-called "false

air" is drawn into the furnace and mixes with the furnace gases.

Blast rate (Nm^3/h)	14000
O$_2$ in air blast (%)	21
Temperature of blast (K)	673
Permeability of the packed bed	0.3
Diameter of particles (m)	0.1
Weight percent of cokes in charge	0.07
Weight percent of PbO containing materials in charge	0.93

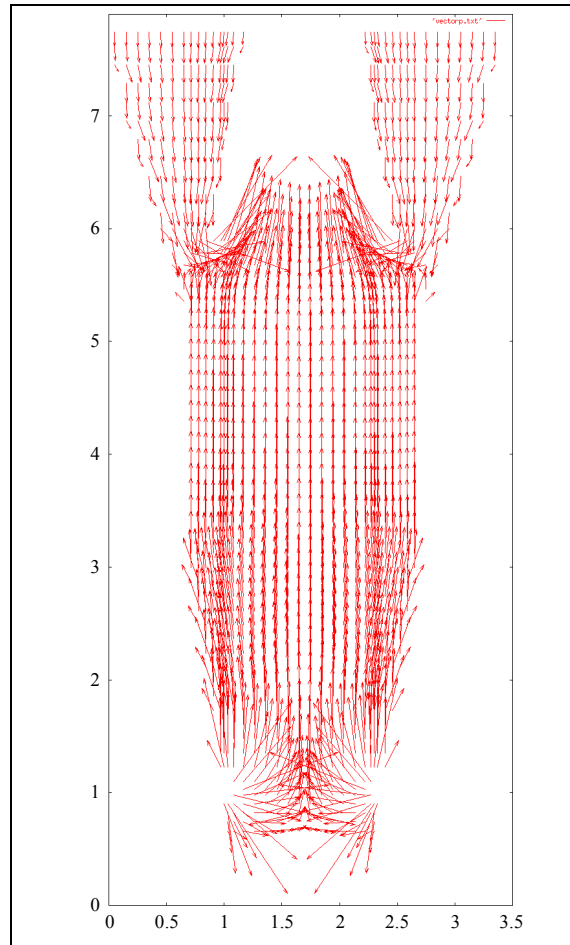**Table 2**: Parameter values and operating conditions for the base case.

Figure 4: Calculated gas flow in the blast furnace for the base case (see table 2).

Figure 5 shows the flow of the solid material in the blast furnace. In the furnace solid material transforms into other phases by melting, reactions, evaporation, etc… This loss of solid material will immediately be compensated by solid material from the neighbouring cells. This is what causes the solid material to flow. Figure 6 shows a detail of the solid flow field in the bottom region of the furnace. As can be seen on the figure, the solid material flows towards the tuyeres. This is the result from the combustion reactions by which large amounts of coke are consumed. The liquid flow field is shown in figure 7. The liquid phase flows straight down except at the wall boundaries. The figure also shows the accumulation of liquid material at inclined boundary walls, resulting in higher mass flow vectors at the bottom sidewalls.

The model also calculates the temperature profiles of the different phases. As an example, figure 8 shows the temperature profile of the gas phase for the base case. As the air enters the furnace the combustion reaction between carbon and oxygen starts immediately. This causes a strong temperature rise in the gas phase. The CO$_2$-gas that is formed by this reaction, reacts further with the carbon to produce CO-gas. As this is an endothermic reaction, the temperature in the center of the furnace is somewhat lower. From the tuyere zone, the gas rises to the exhaust hood and heats up the cold charge. The top of the liquid bath was set as a wall boundary condition for the gas phase, as it is assumed that no gas penetrates the liquid phase.
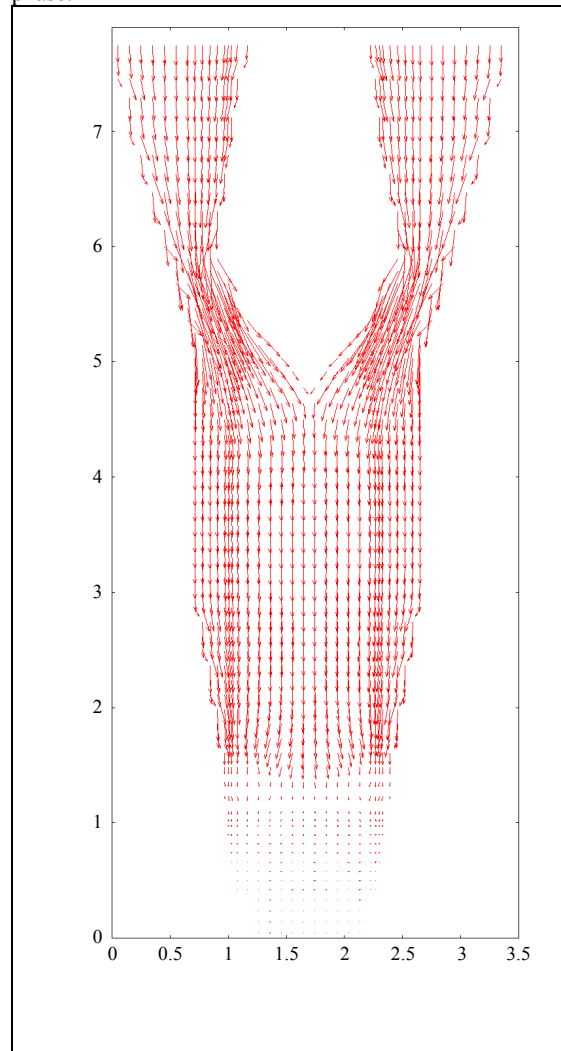

Figure 5: Calculated flow field of solids in the blast furnace for the base case (see table 2).
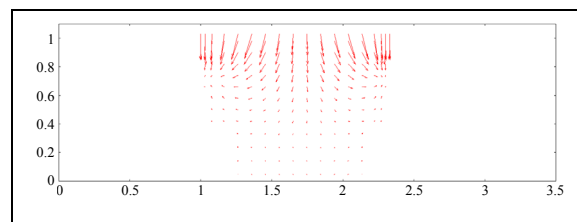

Figure 6: Detail of the solid flow field in the bottom region of the blast furnace for the base case (see table 2).

The composition of the different phases can also be displayed as a result from the model. Figure 9 shows the volume fraction of oxygen in the gas phase. At the tuyeres, a rapid decrease of the oxygen concentration can be seen as a result from the combustion reaction. The figure also shows the false air in the charge bins. In figure 10, the mass fraction of cokes in the furnace is shown. Starting from the charge bins, a small decrease of the coke fraction can be determined up to the melting zone of PbO. This decrease is caused by the Boudouard reaction. In the melting zone, a large increase in coke fraction can be seen. When all the lead oxide is melted, a coke bed remains.
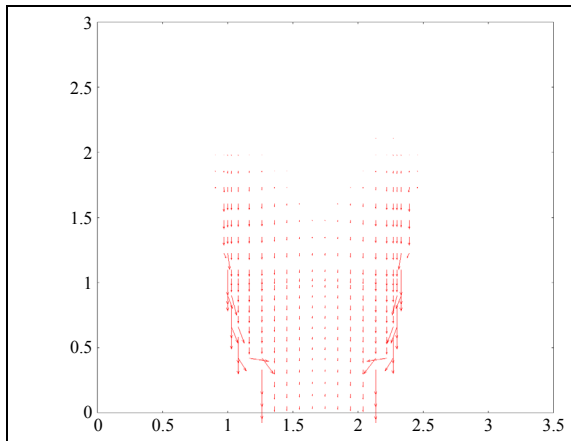

Figure 7: The calculated liquid flow field in the blast furnace for the base case (see table 2).
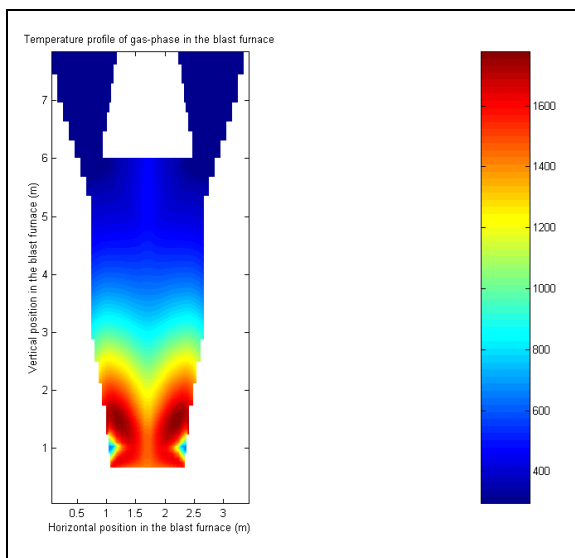

Figure 8: The temperature profile of the gas phase in the blast furnace for the base case (see table 2).
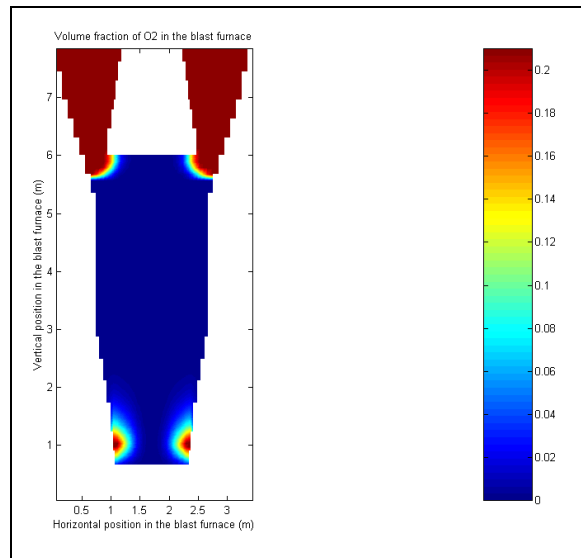

Figure 9: Profile of the volume fraction of O_2 in the gas phase for the base case (see table 2).
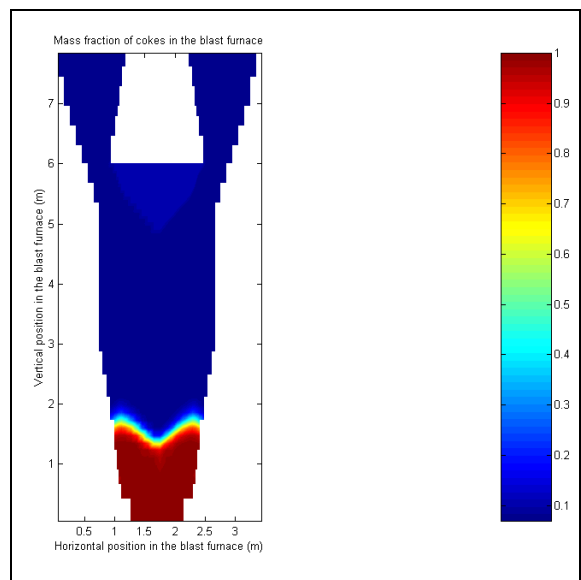

Figure 10: Profile of the mass fraction of cokes in the blast furnace for the base case (see table 2).

In the foregoing paragraphs the different results that can be obtained from the model were presented. The model was furthermore used to investigate the influence of certain operating parameters on blast furnace performance.

Influence of oxygen enrichment

Oxygen enrichment of the blast air is frequently used in blast furnace operation to increase production rate. Since more oxygen enters the furnace, more heat from coke combustion is available to melt the charge. By adding up the amount of solid material that transforms by the reactions, the production rate of the furnace can be calculated. For the base model the total production rate was calculated to be 892 tons/day. When the blast air contains 25 % of oxygen, the production capacity was calculated to be 1063 tons/day. Oxygen enrichment of the blast air has undoubtedly a very beneficial effect on blast furnace performance.

Influence of temperature increase of the blast air

It was presumed that raising the blast air temperature would have little effect on the production rate. To investigate the influence of a temperature increase of the blast air, the blast air temperature was raised to 600 °C with an oxygen content of the blast air at 25 %. The model calculated a production capacity of 1110 tons/day. This result indicates a clear effect of the blast air temperature on production rates. The higher temperature of the gas phase results primarily in higher temperatures of all the phases, mainly in the tuyere zone. Because of the higher temperatures however, the Boudouard rate is faster. This results in higher coke consumption, and thus also a higher melting rate and higher production capacity.

DISCUSSION

With the blast furnace model described in this paper we have shown to be able to describe the global state of the blast furnace (flow fields, temperature profiles, composition profiles…) during operation. The results obtained with regard to oxygen enrichment of the blast air, and increasing the blast air temperature, qualitatively agree with real blast furnace performance. For quantitative analysis, the current model could be further improved for the following points:

- The current solid charge is highly simplified in comparison with a real charge in a lead blast furnace. Also the number of reactions modelled is very limited.
- In the model some physical aspects are currently neglected as for example diffusion of species in the gas phase and thermal radiation.
- A constant diameter is used for the components in the charge.
- The first order upwind scheme that is used for the discretisation of the partial differential equations causes numerical diffusion.
- The currently used grid is rather coarse. Furthermore, the grid consists of rectangular cells that are not boundary fitted on the inclined walls.

Beside the need for further improvement of the model, there is evidently need for a thorough, quantitative evaluation of the model. Frequent probings will be a useful tool for obtaining temperature, pressure and gas composition profiles across the furnace. They can readily be used for comparison between model predictions and operational data.

CONCLUSION

In the paper a two-dimensional steady stade simulation model was presented for a lead blast furnace. The model handles the most important phenomena occurring during the blast furnace process. The results of the simulation model give a clear view on blast furnace operation and qualitatively describe the influence of certain operating parameters on blast furnace performance. Guidelines for improvement of the model have been indicated.

REFERENCES

AKIYAMA, T., YAGI, J., NOGAMI, H. and DE CASTRO, J.A., (2000), "Transient Mathematical Model of Blast Furnace Based on Multi-Fluid Concept", MINPREX 2000, 519-526.

AUSTIN, P.R., NOGAMI, H. and YAGI, J., (1997), "A Mathematical Model for Blast Furnace Reaction Analysis Based on the Four Fluid Model", ISIJ International, **37** (8), 748-755.

CHAO, J.T., (1981), "A dynamic simulation of a lead blast furnace", Metallurgical Transactions B, **12**, 385-402.

COWPERTHWAITE, J.E., DUGDALE, P.J., LANDRY, C.J.F., MORRIS, D.R., STEWARD, F.R. and WILSON, T.C.W., (1980), "Energy Aspects of a Lead Blast Furnace", Metallurgical Transactions B, **11**, 291-299.

DE CASTRO, J.A., NOGAMI, H. and YAGI, J., (2000), "Transient Mathematical Model of Blast Furnace Based on Multi-fluid Concept, with Application to High PCI Operation", ISIJ International, **40** (7), 637-646.

DE CASTRO, J.A., NOGAMI, H. and YAGI, J., (2002),"Three-dimensional Multiphase Mathematical Modeling of the Blast Furnace Based on the Multi-Fluid Model", ISIJ International, **42** (1), 44-52.

HUSSAIN, M.M. and MORRIS, D.R., (1989), "Mathematical model of the stack region of a commercial lead blast furnace", Metallurgical Transactions B, **20**, 97-106.

SHIRAI, T., (1956), ?, Kagaku Kogaku-to-Kagaku Kikai, **1**, 216.

STUKE, B., (1948), "Berechnung des Warmeaustausches in Regeneratoren mit Zylindrischen und Kugelformigen Fullmaterial", Angewandte Chemie, **20**, 262.